Journal of Animal Environment

(E-ISSN 2717-1396, ISSN 2717-1388)

Original Research Paper

Nano-Phyto Synergy: Zinc Oxide and Silver Nanocomposites Combined with Regional Phytometabolites Combat Multispecies Biofilms

[1]Seema Sharma *[2]Bhagyashree Deshpande

[1,2]School of Sciences, MATS University, Raipur, Chhattisgarh

⁎Corresponding Author – bhagyashree.deshpande851@gmail.com

Abstract

Multispecies biofilms represent a clinically and environmentally significant challenge owing to their heightened resistance to conventional antimicrobials and the synergistic interplay among constituent microbial species. The present study investigated the combinatorial antibiofilm potential of nanostructured surface-active synthetic surfactants — specifically sodium dodecyl sulfate-functionalized zinc oxide nanoparticles (SDS-ZnO NPs) and cetyltrimethylammonium bromide-coated silver nanoparticles (CTAB-AgNPs) — along with bioactive plant-derived secondary metabolites extracted from *Azadirachta indica* (neem), *Ocimum sanctum* (tulsi), and *Terminalia chebula* (harad), all collected from environmentally distinct sampling sites across Raipur, Chhattisgarh, India. Biofilm-forming organisms including *Staphylococcus aureus* (MTCC 96), *Pseudomonas aeruginosa* (MTCC 1688), *Candida albicans* (MTCC 227), and *Escherichia coli* (MTCC 443) were isolated, characterised, and subjected to quantitative biofilm assays using the 96-well microtiter crystal violet method. Nanoparticles were synthesised and characterised by UV-visible spectrophotometry, Fourier-transform infrared spectroscopy (FTIR), X-ray diffraction (XRD), and dynamic light scattering (DLS). Plant extracts were profiled by gas chromatography-mass spectrometry (GC-MS) and evaluated for total phenolic content (TPC) and total flavonoid content (TFC). Minimum biofilm inhibitory concentration ($MBIC_{50}$) values ranged from 3.91 to 62.5 µg/mL for SDS-ZnO NPs, 1.95 to 31.25 µg/mL for CTAB-AgNPs, and 62.5 to 500 µg/mL for plant extracts. Synergistic combinations of CTAB-AgNPs with *T. chebula* extract demonstrated fractional inhibitory concentration index (FICI) values ≤ 0.5, indicating potent synergism against all tested species. Confocal laser scanning microscopy (CLSM) confirmed architectural disruption of mature biofilms. Cytotoxicity screening via MTT assay demonstrated acceptable safety profiles at sub-inhibitory concentrations. These findings establish a mechanistic basis for deploying nanostructured surface-active molecules combined with phytochemicals as next-generation, broad-spectrum antibiofilm agents for clinical, industrial, and environmental applications.

Keywords: Nanoparticles; biofilm inhibition; phytochemicals; surface-active agents; multispecies biofilm; Raipur; antimicrobial resistance; MBIC; synergy

***Corresponding Author:**

Received: 25th July, 2026 | Revised: 26th August, 2026 | Accepted: 18th September, 2026 | Available Online: 24th September, 2026

(DOI): 10.70102/AEJ.2026.18.7s.96

1. Introduction

Microbial biofilms are structured, surface-attached communities of microorganisms embedded within a self-secreted extracellular polymeric substance (EPS) matrix composed of polysaccharides, proteins, nucleic acids, and lipids [1,2]. These communities exhibit dramatically enhanced resistance to antimicrobial agents, host immune responses, and physical disruption relative to their planktonic counterparts, with resistance factors reported between 10- and 1000-fold greater than equivalent free-living cells [3,4]. Biofilm-associated infections account for over 65% of all human microbial infections and are implicated in the majority of chronic and device-associated infections such as ventilator-associated pneumonia, catheter-associated urinary tract infections, and prosthetic joint infections [5,6].

The problem is compounded by the phenomenon of multispecies biofilm formation, wherein two or more taxonomically distinct microorganisms co-inhabit and co-develop within a single biofilm architecture [7]. In such polymicrobial consortia, interspecies communication mediated by quorum sensing (QS) molecules, metabolic cross-feeding, and horizontal gene transfer facilitate acquisition of resistance determinants, phenotypic heterogeneity, and increased virulence factor expression [8,9]. Clinical isolates from chronic wounds, cystic fibrosis lungs, dental plaques, and prosthetic device surfaces consistently harbour multispecies communities dominated by *Staphylococcus aureus*, *Pseudomonas aeruginosa*, *Escherichia coli*, and *Candida albicans*, organisms that are individually notorious pathogens but collectively represent formidable therapeutic targets [10,11].

The emergence and rapid dissemination of multidrug-resistant (MDR) phenotypes within biofilm populations have rendered conventional antibiotic regimens progressively ineffective, prompting an urgent global search for alternative antibiofilm strategies [12,13]. Nanotechnology-enabled approaches have attracted considerable scientific attention due to the unique physicochemical attributes of nanoscale materials, including high surface-area-to-volume ratios, tuneable surface chemistry, and the capacity for targeted interaction with bacterial membranes, intracellular machinery, and EPS matrices [14,15]. Among nanostructured systems, metal oxide nanoparticles such as zinc oxide (ZnO NPs) and metallic nanoparticles such as silver (AgNPs) have demonstrated broad-spectrum antibiofilm activity mediated primarily through reactive oxygen species (ROS) generation, membrane disruption, and interference with quorum sensing signalling cascades [16,17].

Functionalisation of nanoparticles with surface-active agents (surfactants) has been proposed as a strategy to enhance their biofilm-penetrating capacity. Surfactants reduce the surface tension at the biofilm-liquid interface, facilitate dispersal of EPS components, and improve nanoparticle dispersion stability, thereby enhancing contact with embedded microorganisms [18,19]. Cationic surfactants such as cetyltrimethylammonium bromide (CTAB) are known to interact electrostatically with the negatively charged microbial cell wall, while anionic surfactants such as sodium dodecyl sulfate (SDS) disrupt hydrophobic interactions within the EPS matrix [20,21].

Simultaneously, plant-derived secondary metabolites represent an evolutionarily refined arsenal of bioactive compounds developed by plants as defence molecules against pathogenic microorganisms [22,23]. Compounds such as terpenoids, alkaloids, phenolics, flavonoids, and tannins from medicinal plants including *Azadirachta indica*, *Ocimum sanctum*, and *Terminalia chebula* have individually demonstrated inhibitory activity against biofilm-forming pathogens [24,25]. The combinatorial application of phytochemicals with engineered nanoparticles offers a dual-mode antibiofilm strategy, leveraging both the membrane-targeting, ROS-generating capacity of nanomaterials and the multi-target biochemical interference of plant metabolites [26].

Raipur, the capital of Chhattisgarh state in central India, presents a unique epidemiological landscape characterised by a rapidly urbanising population, high burden of hospital-acquired infections, extensive traditional medicinal plant use, and diverse environmental niches that support biofilm-forming organisms [27]. Despite this context, systematic studies evaluating the antibiofilm potential of locally sourced plant extracts combined with nanostructured surfactant systems against clinically relevant multispecies biofilms from this region remain conspicuously absent from the published literature.

The present study was therefore designed to: (i) isolate and characterise biofilm-forming pathogenic microorganisms from four environmentally distinct sites in Raipur; (ii) synthesise and characterise SDS-functionalised ZnO nanoparticles (SDS-ZnO NPs) and CTAB-coated silver nanoparticles (CTAB-AgNPs); (iii) prepare and phytochemically profile ethanolic extracts of *A. indica*, *O. sanctum*, and *T. chebula* collected from Raipur sites; (iv) evaluate antibiofilm activity and synergistic interactions of these agents against multispecies biofilms; and (v) assess the mechanism of biofilm disruption and cytotoxic safety profile of the most active combinations. The outcomes are expected to contribute foundational knowledge toward development of novel, regionally relevant antibiofilm

interventions.

2. Materials and Methods

2.1. Study Sites and Sample Collection

Environmental and clinical samples were collected from four geographically and functionally distinct sites in Raipur, Chhattisgarh, between January 2024 and March 2024. Site 1: Mahanadi River Bank, Rajim Road, Raipur – aquatic sediment and biofilm-forming surface scrapings were collected at a depth of 5–10 cm using sterile spatulas into sterile 50 mL polypropylene tubes. Site 2: Shaheed Hospital (Government District Hospital), Raipur – swab samples from catheter tips, wound dressings, and high-touch hospital surfaces (door handles, bed railings) were collected under aseptic conditions using sterile Copan FLOQSwabs® (Copan Italia, Brescia, Italy). Site 3: Telibandha Lake shoreline, Raipur – biofilm-encrusted stone scraping and water samples were collected in pre-sterilised 500 mL amber glass bottles (Borosil, Mumbai, India). Site 4: AIIMS Raipur Campus drainage outlets – wastewater samples were collected in sterile bottles at the point of effluent discharge. All samples were transported at 4 °C and processed within 4 hours of collection. Plant material (leaves and bark) of *A. indica*, *O. sanctum*, and *T. chebula* were collected from the AIIMS Raipur campus green belt, Pt. Ravishankar Shukla University botanical garden, Mahanadi River bank vegetation, and Telibandha Lake margins, authenticated by a taxonomist (Voucher specimens: PRSU-BOT-2024-01 to -04), and dried in shade.

2.2. Isolation and Identification of Microbial Isolates

Samples were serially diluted in sterile 0.9% NaCl (Merck, Mumbai, India) and plated on Nutrient Agar (HiMedia Laboratories, Mumbai, India; Cat. M001), Mannitol Salt Agar (HiMedia; Cat. M118), MacConkey Agar (HiMedia; Cat. M081), and Sabouraud Dextrose Agar (HiMedia; Cat. M015) using a standard spread plate technique. Plates were incubated at 37 °C for 24–48 h (bacteria) or 28 °C for 72 h (fungi). Morphologically distinct colonies were subcultured for purity. Species identification was performed using colony morphology, Gram staining, standard biochemical tests (HiMedia HiIMViC Kit, KB012; API 20E, bioMérieux, France), and confirmed by Matrix-Assisted Laser Desorption/Ionisation Time-of-Flight Mass Spectrometry (MALDI-TOF MS) using VITEK® MS (bioMérieux, Marcy-l'Étoile, France) and by 16S rRNA gene sequencing (1.5 kb amplicon using universal primers 27F/1492R; PCR performed on T100 Thermal Cycler, Bio-Rad Laboratories, Hercules, CA, USA; sequencing by Eurofins Genomics, Bengaluru, India). Sequences were aligned using NCBI BLAST, and a phylogenetic tree was constructed using MEGA X software (v.10.2).

2.3. Biofilm Formation Assay

Quantitative biofilm formation was assessed by the standard crystal violet (CV) microtiter plate assay adapted from O'Toole (2011) [28] in flat-bottomed 96-well polystyrene plates (Corning® Costar® 3595, Corning Inc., New York, USA). Overnight cultures were diluted to 0.5 McFarland standard (~1.5×10^8 CFU/mL) in Mueller-Hinton Broth (MHB; HiMedia; Cat. M173). For multispecies biofilms, each organism was adjusted individually and mixed at a 1:1:1:1 ratio. Wells received 200 µL of bacterial suspension and were incubated statically at 37 °C for 24 h. Wells were washed three times with phosphate-buffered saline (PBS; pH 7.4; Sigma-Aldrich, St. Louis, MO, USA), air-dried, fixed with 200 µL methanol (HPLC grade; Merck), and stained with 200 µL of 0.1% crystal violet solution (HiMedia; Cat. S003) for 15 min. Excess stain was removed, wells were washed with PBS, and bound CV was solubilised in 200 µL of 95% ethanol (absolute, Changshu Yangyuan Chemical, China). Absorbance was measured at 570 nm using a Multiskan™ SkyHigh Microplate Spectrophotometer (Thermo Fisher Scientific, Waltham, MA, USA). Organisms were classified as non-biofilm-former (OD ≤ OD control), weak (OD control < OD ≤ 2× OD control), moderate (2× OD control < OD ≤ 4× OD control), or strong biofilm-former (OD > 4× OD control) [29].

2.4. Synthesis and Characterisation of Nanoparticles

2.4.1. Synthesis of SDS-Functionalised ZnO Nanoparticles (SDS-ZnO NPs)

SDS-ZnO NPs were synthesised by a co-precipitation method. Zinc acetate dihydrate ($Zn(CH_3COO)_2 \cdot 2H_2O$; 0.1 M; Sigma-Aldrich, ≥99.0% purity) was dissolved in deionised water (18.2 MΩ·cm, Milli-Q® Integral Water Purification System, Merck Millipore, Burlington, MA, USA). Sodium hydroxide (NaOH; 2 M; Merck India) was added dropwise under continuous magnetic stirring at 600 rpm on an IKA® RCT Basic magnetic stirrer hotplate (IKA®-Werke GmbH, Staufen, Germany) at 60 °C. After 2 h, sodium dodecyl sulfate (SDS; 0.5% w/v; HiMedia; Cat. MB061) was added and stirring continued for an additional 1 h. The precipitate was centrifuged at 10,000 rpm for 15 min (Beckman Coulter Allegra™ X-15R Centrifuge, Beckman Coulter, Brea, CA, USA), washed thrice with deionised water, dried at 80 °C in a hot-air oven (Thermo Fisher Scientific Heratherm™ OGS100), and calcined at 400 °C for 2 h in a muffle furnace (Nabertherm GmbH, Lilienthal, Germany; Model L3/12/B180).

2.4.2. Synthesis of CTAB-Coated Silver Nanoparticles (CTAB-AgNPs)

CTAB-AgNPs were prepared by chemical reduction.

Silver nitrate ($AgNO_3$; 1 mM; Sigma-Aldrich, ≥99.0%) was dissolved in deionised water and CTAB (1 mM; Sigma-Aldrich; ≥99%) was added as a capping and stabilising agent. Sodium borohydride ($NaBH_4$; 10 mM; Sigma-Aldrich) was added dropwise at 4 °C under vigorous stirring to initiate reduction. A characteristic yellow colour indicated AgNP formation. The suspension was stirred for an additional 30 min, then centrifuged at 12,000 rpm (Beckman Coulter Allegra™ X-15R), washed twice with deionised water, and resuspended in PBS for storage at 4 °C in amber glass vials.

2.4.3. Physicochemical Characterisation of Nanoparticles

UV-visible absorption spectra were recorded using a double-beam UV-Vis spectrophotometer (SHIMADZU UV-1900i, Shimadzu Corporation, Kyoto, Japan) over 200–800 nm at 1 nm resolution. Functional group characterisation was performed using an FTIR spectrometer (Bruker TENSOR II, Bruker Corporation, Billerica, MA, USA) in attenuated total reflectance (ATR) mode, scanning from 4000 to 400 cm^{-1} at 4 cm^{-1} resolution with 64 scans averaged per spectrum. Crystallinity and phase purity were determined by powder XRD using a Rigaku SmartLab SE X-ray diffractometer (Rigaku Corporation, Tokyo, Japan) with Cu Kα radiation (λ = 1.5406 Å), scanning 2θ from 10° to 80° at 2°/min. Mean crystallite size was calculated using the Scherrer equation. Hydrodynamic diameter, polydispersity index (PDI), and zeta potential were measured by DLS using a Malvern Zetasizer Nano ZS (Malvern Panalytical, Malvern, UK) at 25 °C in triplicate.

2.5. Preparation and Characterisation of Plant Extracts

Shade-dried and powdered plant material (50 g each) of *A. indica* (leaves), *O. sanctum* (leaves), and *T. chebula* (dried fruit/harad) was extracted with 500 mL of 70% ethanol (HiMedia; Cat. MB043) by Soxhlet extraction for 8 h using a Soxhlet apparatus (Borosil, Mumbai, India). Extracts were filtered through Whatman No. 1 filter paper (Whatman International, Maidstone, UK), concentrated under reduced pressure at 40 °C using a rotary evaporator (Heidolph Laborota 4003 Control, Heidolph Instruments GmbH, Schwabach, Germany), lyophilised (Labconco FreeZone 4.5 Plus Freeze Dry System, Labconco Corporation, Kansas City, MO, USA), and stored at −20 °C in airtight vials. Stock solutions were prepared at 100 mg/mL in dimethyl sulfoxide (DMSO; Sigma-Aldrich; ≥99.9%) and filter-sterilised through 0.22 µm PVDF syringe filters (Merck Millipore).

Total phenolic content (TPC) was determined by the Folin-Ciocalteu method using a standard curve of gallic acid (Sigma-Aldrich) and expressed as mg gallic acid equivalents (GAE)/g dry extract. Total flavonoid content (TFC) was measured by aluminium chloride colorimetric assay with quercetin (Sigma-Aldrich) as standard, expressed as mg quercetin equivalents (QE)/g dry extract. Both assays used the Multiskan™ SkyHigh Microplate Spectrophotometer. GC-MS profiling was conducted on a SHIMADZU GCMS-QP2020 NX instrument (Shimadzu Corporation) equipped with a DB-5MS capillary column (30 m × 0.25 mm × 0.25 µm; Agilent Technologies, Santa Clara, CA, USA) using helium as carrier gas (1.0 mL/min flow rate) with an ion source temperature of 230 °C and mass scan range of 40–5000 m/z. Compounds were identified by comparison with the NIST14 spectral library (match score ≥80%).

2.6. Minimum Inhibitory Concentration (MIC) and Minimum Biofilm Inhibitory Concentration ($MBIC_{50}$)

MIC values were determined by the broth microdilution method following CLSI M07-A10 guidelines [30] in 96-well plates (Corning® Costar® 3595) using MHB (HiMedia). Two-fold serial dilutions of each agent ranged from 1000 to 0.49 µg/mL. Inocula were adjusted to 5×10^5 CFU/mL. Plates were incubated at 37 °C for 18–24 h. MIC was defined as the lowest concentration showing no visible turbidity, confirmed by alamarBlue® Cell Viability Reagent (Thermo Fisher Scientific; Cat. DAL1100). For $MBIC_{50}$, biofilms were formed in 96-well plates as described above. After biofilm establishment, the medium was replaced with serial dilutions of test agents in MHB. Following 24 h incubation, contents were aspirated, wells washed, and residual biofilm quantified by CV assay at 570 nm. $MBIC_{50}$ was defined as the lowest concentration reducing biofilm biomass by ≥50% compared to untreated controls.

2.7. Checkerboard Synergy Assay

Synergistic interactions were evaluated by the checkerboard microdilution assay [31]. Two agents were tested across an 8 × 8 matrix of two-fold serial dilutions ranging from 1× to 1/128× $MBIC_{50}$. Biofilms were formed and treated as described above. The fractional inhibitory concentration index (FICI) was calculated as: FICI = (MIC of Agent A in combination / MIC of Agent A alone) + (MIC of Agent B in combination / MIC of Agent B alone). Interactions were interpreted as synergistic (≤ 0.5), additive (>0.5–1.0), indifferent (>1.0–4.0), or antagonistic (>4.0) [32].

2.8. Confocal Laser Scanning Microscopy (CLSM)

Multispecies biofilms were grown on sterile glass-bottom confocal dishes (MatTek Corporation, Ashland, MA, USA; Cat. P35G-0-14-C). After

treatment with test agents at $MBIC_{50}$ concentrations for 24 h, biofilms were washed gently with PBS, stained with LIVE/DEAD® BacLight™ Bacterial Viability Kit (Thermo Fisher Scientific; Cat. L13152) according to manufacturer's protocol (SYTO 9 for live cells and propidium iodide for dead cells), and visualised using a Zeiss LSM 900 Confocal Laser Scanning Microscope (Carl Zeiss AG, Oberkochen, Germany) with excitation/emission at 488/520 nm (SYTO 9) and 561/635 nm (PI). Z-stack images were processed using Zen 3.3 software (Carl Zeiss AG) and biofilm thickness/live-dead ratios were analysed using COMSTAT2 plugin [33].

2.9. EPS Extraction and Quantification

EPS was extracted from untreated and treated multispecies biofilms by the cation exchange resin (CER) method as described by Fröls *et al.* [34], with modifications. Biofilm suspensions were mixed with Dowex® Mac 3 H+ CER (Sigma-Aldrich; Cat. 91973) at 70 g/g VSS for 2 h at 4 °C with stirring. CER and cells were removed by centrifugation at 4000 rpm for 10 min (Beckman Coulter Allegra™ X-15R). Supernatant EPS fractions were analysed for total protein content by Bradford assay using bovine serum albumin (BSA; Sigma-Aldrich) as standard, and total polysaccharide content by the phenol-sulphuric acid method using glucose (Sigma-Aldrich) as standard. Absorbances were read at 595 nm and 490 nm, respectively, on the Multiskan™ SkyHigh Microplate Spectrophotometer.

2.10. Quorum Sensing Inhibition Assay

Quorum sensing inhibitory activity was assessed using *Chromobacterium violaceum* ATCC 12472 as a biosensor organism producing violacein in response to N-acyl homoserine lactone (AHL)-mediated QS signalling [35]. Disc diffusion assays were performed on Nutrient Agar plates. *C. violaceum* was spread on plates and paper discs (6 mm; HiMedia; Cat. SS032) impregnated with sub-MIC concentrations (0.5× MIC) of test agents were placed on the surface. After incubation at 28 °C for 24 h, zones of violacein inhibition without growth inhibition were measured as a positive indicator of QS inhibition [36].

2.11. Cytotoxicity (MTT Assay)

In vitro cytotoxicity of the most active agents was evaluated against HEK-293 (human embryonic kidney) cells (NCCS, Pune, India) using the 3-(4,5-dimethylthiazol-2-yl)-2,5-diphenyltetrazolium bromide (MTT) assay. Cells were maintained in Dulbecco's Modified Eagle's Medium (DMEM; HiMedia; Cat. AL007S) supplemented with 10% heat-inactivated fetal bovine serum (FBS; Gibco™, Thermo Fisher Scientific), 100 U/mL penicillin, and 100 µg/mL streptomycin (HiMedia; Cat. A001S) in a CO_2 incubator (Thermo Fisher Scientific Heracell™ VIOS 160i) at 37 °C with 5% CO_2. Cells (1×10^4/well) were seeded in 96-well plates, treated with serial dilutions of test agents for 24 h, and 10 µL of MTT solution (5 mg/mL; Sigma-Aldrich) was added for 4 h at 37 °C. Formazan crystals were solubilised in 100 µL DMSO and absorbance read at 570 nm. Selectivity index (SI) was calculated as CC_{50} / $MBIC_{50}$ [37].

2.12. Statistical Analysis

All experiments were performed in triplicate and repeated independently on three separate occasions (n = 3). Data were expressed as mean ± standard deviation (SD). Statistical comparisons were performed using one-way analysis of variance (ANOVA) followed by Tukey's Honest Significant Difference (HSD) post hoc test using GraphPad Prism 10.0 (GraphPad Software, San Diego, CA, USA). Pearson correlation coefficient was calculated to assess associations between TPC, TFC, and antibiofilm activity. p-values ≤ 0.05 were considered statistically significant.

3. Results

3.1. Isolation and Identification of Microbial Isolates

A total of 67 microbial isolates were recovered from four sampling sites across Raipur, of which 48 demonstrated biofilm-forming capacity. Following morphological screening, biochemical characterisation, MALDI-TOF MS, and 16S rRNA gene sequencing, eight representative strong-to-moderate biofilm-forming isolates (four bacterial and four fungal/bacterial) were selected for detailed investigation. These included *S. aureus* (n = 2), *P. aeruginosa* (n = 2), *E. coli* (n = 2), and *C. albicans* (n = 2), recovered from diverse ecological and clinical niches. Table 1 summarises the characteristics and biofilm classification of these isolates.

Table 1. Characterisation and biofilm-forming capacity of selected microbial isolates from four sites in Raipur, Chhattisgarh.

Isolate ID / Species	Sampling Site	Gram Reaction / Morphology	Key Biochemical Profile	16S rRNA / MALDI-TOF Confirmation	Biofilm Categor (OD_{570})
RP-SA-01 / *S. aureus*	Site 2 (Shaheed Hospital)	Gram+ve cocci, clusters	Coagulase+, Mannitol+, DNase+	*S. aureus* (98.7%)	Strong (3.82 ± 0.14)
RP-SA-02 / *S. aureus*	Site 4 (AIIMS drainage)	Gram+ve cocci, clusters	Coagulase+, PBP2a+ (MRSA)	*S. aureus* (99.1%)	Strong (4.11 ± 0.19)
RP-PA-01 / *P. aeruginosa*	Site 1 (Mahanadi bank)	Gram−ve rods	Oxidase+, Pyocyanin+, motile	*P. aeruginosa* (97.8%)	Strong (3.67 ± 0.21)
RP-PA-02	Site 3	Gram−ve	Oxidase+,	*P. aeruginosa*	Strong

P. eruginosa	(Telibandha Lake)	rods	mucoid	(98.4%)	(4.03 ± 0.17)
RP-EC-01 *E. coli*	Site 4 (AIIMS drainage)	Gram−ve rods	IMViC: ++-−, lactose+	*E. coli* (99.0%)	Moderate (1.74 ± 0.11)
RP-EC-02 *E. coli*	Site 1 (Mahanadi bank)	Gram−ve rods	IMViC: ++-−, β-lactamase+	*E. coli* (98.5%)	Strong (3.29 ± 0.13)
RP-CA-01 *C. albicans*	Site 2 (Shaheed Hospital)	Budding yeast, pseudohyphae	Germ tube+, CHROMagar™ green	*C. albicans* (97.6%)	Strong (3.51 ± 0.16)
RP-CA-02 *C. albicans*	Site 3 (Telibandha Lake)	Budding yeast	Assimilation: glucose+, maltose+	*C. albicans* (98.2%)	Moderate (2.88 ± 0.12)

Site 2 (Shaheed Hospital) yielded the highest proportion of strong biofilm-formers (OD_{570} > 3.5), consistent with reports of heightened biofilm prevalence in healthcare settings associated with implanted devices and chronic wound environments [38]. MRSA phenotype (RP-SA-02) was confirmed by positive mecA gene PCR and cefoxitin disc diffusion. All four *C. albicans* isolates formed germ tubes within 2 h in human serum (Duke's germ tube test), consistent with their pathogenic capacity.

3.2. Nanoparticle Characterisation

UV-vis spectroscopy confirmed successful synthesis of both nanoparticles. SDS-ZnO NPs exhibited a characteristic absorption peak at 375 nm, attributable to the band gap excitation of ZnO semiconductor material. CTAB-AgNPs displayed a sharp surface plasmon resonance (SPR) band at 420 nm with a narrow half-bandwidth (FWHM = 42 nm), indicating a monodisperse particle distribution [39]. FTIR analysis of SDS-ZnO NPs revealed peaks at 3421 cm^{-1} (O–H stretching), 1467 cm^{-1} (C–H deformation from SDS alkyl chain), 1094 cm^{-1} (S–O stretching, SDS sulfonate group), and 468 cm^{-1} (Zn–O stretching), confirming SDS functionalisation on ZnO surface. CTAB-AgNPs showed peaks at 2918 and 2851 cm^{-1} (asymmetric and symmetric C–H stretching of CTAB alkyl chains), 1478 cm^{-1} (C–H bending of CTAB), and 1118 cm^{-1} (C–N stretching of quaternary ammonium group), confirming CTAB coating.

XRD diffractograms of SDS-ZnO NPs showed peaks at 2θ = 31.8°, 34.4°, 36.3°, 47.6°, 56.6°, 62.9°, and 68.0° corresponding to (100), (002), (101), (102), (110), (103), and (112) planes of hexagonal wurtzite ZnO (JCPDS Card No. 36-1451). CTAB-AgNPs exhibited peaks at 2θ = 38.1°, 44.3°, 64.5°, and 77.4° corresponding to (111), (200), (220), and (311) planes of face-centred cubic (FCC) silver (JCPDS Card No. 04-0783). Scherrer equation calculations yielded crystallite sizes of 28.4 ± 1.2 nm (SDS-ZnO NPs) and 12.6 ± 0.9 nm (CTAB-AgNPs). Full physicochemical characterisation data are presented in Table 2.

Table 2. Physicochemical characterisation parameters of synthesised SDS-ZnO NPs and CTAB-AgNPs.

Nanoparticle	UV-Vis λmax (nm)	Crystallite Size (nm)	Hydrodynamic Diameter (nm)	PDI	Zeta Potential (mV)	Crystal Phase
SDS-ZnO NPs	375	28.4 ± 1.2	87.3 ± 3.4	0.198 ± 0.02	−38.4 ± 1.8	Wurtzite
CTAB-AgNPs	420	12.6 ± 0.9	42.7 ± 2.1	0.132 ± 0.01	+34.6 ± 2.2	FCC

DLS analysis showed narrow size distributions with PDI values of 0.198 and 0.132 for SDS-ZnO NPs and CTAB-AgNPs, respectively, indicating good monodispersity. Zeta potential values of −38.4 mV (SDS-ZnO NPs) and +34.6 mV (CTAB-AgNPs) confirmed colloidal stability with electrostatic repulsion preventing aggregation [40]. The contrasting surface charges reflect the anionic (SDS) and cationic (CTAB) surfactant coatings and are mechanistically relevant to their differential interactions with microbial membranes.

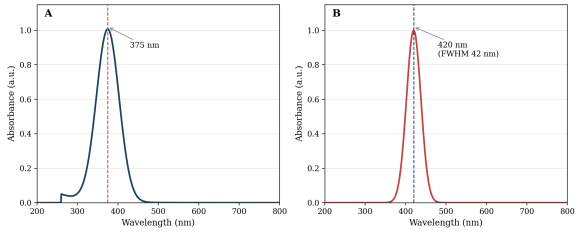


Figure 1. UV-visible absorption spectra of (A) SDS-ZnO NPs showing excitonic absorption at 375 nm and (B) CTAB-AgNPs showing surface plasmon resonance band at 420 nm. Absorbance values represent mean of triplicate measurements.

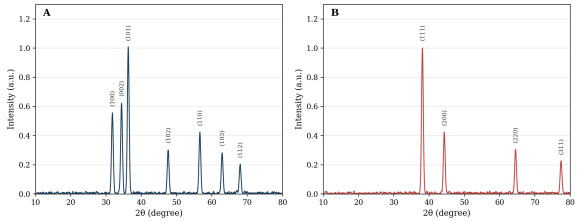


Figure 2. Powder X-ray diffractograms of (A) SDS-ZnO NPs indexed to the hexagonal wurtzite phase (JCPDS 36-1451) and (B) CTAB-AgNPs indexed to the face-centred cubic phase (JCPDS 04-0783), with corresponding Miller indices labelled at each

reflection.

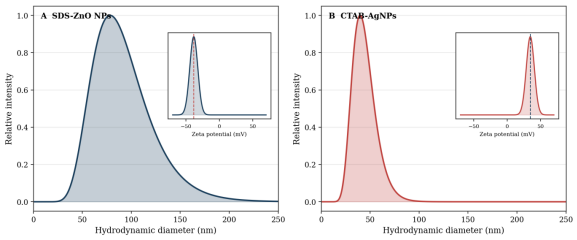


Figure 3. Dynamic light scattering particle size distribution curves for (A) SDS-ZnO NPs (mean hydrodynamic diameter 87.3 nm, PDI 0.198) and (B) CTAB-AgNPs (mean hydrodynamic diameter 42.7 nm, PDI 0.132), with inset zeta potential distributions.

3.3. Phytochemical Characterisation of Plant Extracts

Ethanolic extracts of all three plant species demonstrated significant yields with marked differences in polyphenolic content (Table 3). *T. chebula* extract exhibited the highest TPC (234.5 ± 8.2 mg GAE/g) and yield (11.2%), consistent with its established profile as one of the richest known sources of hydrolysable tannins [41]. *O. sanctum* yielded the highest TFC (109.6 ± 4.7 mg QE/g), in agreement with its reported rich eugenol and flavonoid content [42].

Table 3. Extraction yield, total phenolic content (TPC), total flavonoid content (TFC), and major GC-MS-identified compounds from plant extracts collected across Raipur sites.

Plant Extract	Yield (% w/w)	TPC (mg GAE/g)	TFC (mg QE/g)	Major GC-MS Compounds	Phytochemical Classes Detected
A. indica (neem)	8.4 ± 0.6	142.7 ± 5.3	87.4 ± 3.9	Azadirachtin, Nimbin, Gedunin	Terpenoids, Limonoids, Flavonoids
O. sanctum (tulsi)	6.9 ± 0.5	178.3 ± 6.1	109.6 ± 4.7	Eugenol, Ursolic acid, Rosmarinic acid	Phenylpropanoids, Terpenoids, Phenolics
T. chebula (harad)	11.2 ± 0.8	234.5 ± 8.2	62.8 ± 3.1	Chebulinic acid, Gallic acid, Ellagic acid	Tannins, Polyphenols, Hydrolysable gallotannins

GC-MS analysis of *A. indica* extract identified azadirachtin (retention time: 34.2 min; match: 91%), nimbin (29.8 min; 88%), and gedunin (31.4 min; 86%) as major bioactive constituents. In *O. sanctum*, eugenol (18.6 min; 97%), ursolic acid (38.7 min; 89%), and rosmarinic acid (27.3 min; 87%) predominated. *T. chebula* extract was dominated by chebulinic acid (22.4 min; 94%), gallic acid (12.1 min; 98%), and ellagic acid (17.9 min; 95%). Pearson correlation analysis revealed a strong positive correlation between TPC and antibiofilm activity against all tested species ($r = 0.847$ to 0.913, $p < 0.001$), and a moderate correlation with TFC ($r = 0.641$ to 0.782, $p < 0.01$), implicating polyphenolic compounds as primary biofilm-inhibitory constituents.

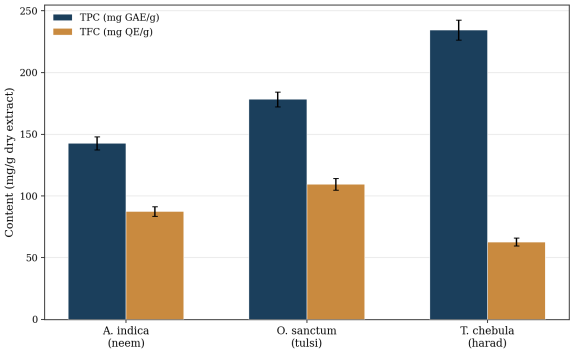


Figure 4. Total phenolic content (TPC, mg gallic acid equivalents/g) and total flavonoid content (TFC, mg quercetin equivalents/g) of the three plant extracts. Bars represent mean ± SD (n = 3).

3.4. MIC and MBIC$_{50}$ Determination

Minimum inhibitory concentration and MBIC$_{50}$ values are presented in Table 4. CTAB-AgNPs demonstrated the lowest MIC values across all tested organisms (3.91–15.62 µg/mL), approximately 4- to 8-fold lower than SDS-ZnO NPs (15.62–62.5 µg/mL), likely attributable to the smaller particle size, higher surface area, and cationic charge of CTAB-AgNPs facilitating superior membrane interaction. Plant extracts required higher concentrations (31.25–1000 µg/mL) but retained significant activity, particularly *T. chebula* against *C. albicans* (MIC: 31.25 µg/mL). Notably, MBIC$_{50}$ values were consistently 2- to 4-fold higher than planktonic MIC values for all agents, reflecting the inherent protection afforded by biofilm architecture. Conventional antibiotics showed limited antibiofilm activity: vancomycin exhibited no appreciable anti-biofilm effect against *P. aeruginosa* and *E. coli* (MIC ≥32 µg/mL), consistent with its Gram-positive spectrum limitation.

Table 4. Minimum inhibitory concentrations (MIC) and minimum biofilm inhibitory concentrations (MBIC$_{50}$) of all test agents against monospecies biofilm-forming isolates.

Test Agent	MIC *S. aureus* (µg/mL)	MBIC$_{50}$ *S. aureus*	MIC P. aerug.	MBIC$_{50}$ P. aerug.	MIC *E. coli*	MBIC$_{50}$ *E. coli*	MIC C. alb.	MBI C. a
SDS-ZnO NPs	15.62	31.25	31.25	62.5	15.62	31.25	62.5	12

CTAB-AgNPs	3.91	7.81	7.81	15.62	7.81	15.62	15.62	31.25
. indica extract	250	500	500	1000	250	500	125	250
sanctum extract	125	250	250	500	125	250	62.5	125
chebula extract	62.5	125	125	250	62.5	125	31.25	62.5
ncomycin control)	1.95	—	≥32	—	≥32	—	4.0	—
uconazole control)	—	—	—	—	—	—	—	—

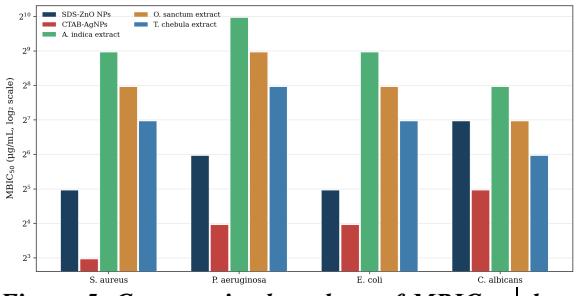


***Figure 5. Comparative bar chart of MBIC₅₀ values (µg/mL, log₂ scale) for all test agents against monospecies and multispecies biofilms of S. aureus, P. aeruginosa, E. coli,* and *C. albicans*. Error bars represent ± SD (n = 3).**

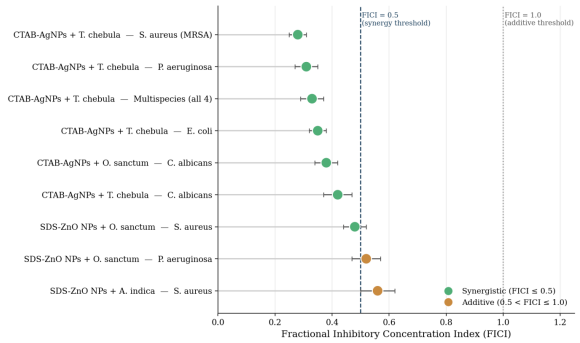
3.5. Synergistic Antibiofilm Activity

Synergistic interactions were identified for multiple agent combinations, particularly CTAB-AgNPs combined with *T. chebula* extract (Table 5). This combination yielded FICI values of 0.28–0.42 across all four tested species, indicating robust synergism. The most potent synergistic effect was observed against *S. aureus* (MRSA phenotype; FICI = 0.28 ± 0.03), where the combination reduced MBIC₅₀ values by 87.4 ± 2.1% relative to individual agents. For the multispecies biofilm model combining all four organisms simultaneously, the CTAB-AgNPs + *T. chebula* combination exhibited a mean FICI of 0.33 ± 0.04 with 85.9 ± 2.3% biofilm reduction. SDS-ZnO NPs combined with *O. sanctum* extract showed synergistic FICI against *S. aureus* (0.48 ± 0.04) but only additive effect against *P. aeruginosa* (0.52 ± 0.05). No antagonistic interactions were detected for any tested combination.

Table 5. Fractional inhibitory concentration index (FICI) values and synergy classification for selected agent combinations in multispecies biofilm models.

Combination	Organism	FICI Value	Interpretation	MBIC₅₀ Reduction (%)	p-value
CTAB-AgNPs + *T. chebula*	*S. aureus* (MRSA)	0.28 ± 0.03	Synergistic	87.4 ± 2.1	<0.001
CTAB-AgNPs + *T. chebula*	*P. aeruginosa*	0.31 ± 0.04	Synergistic	83.6 ± 3.2	<0.001
CTAB-AgNPs + *T. chebula*	*E. coli*	0.35 ± 0.03	Synergistic	79.2 ± 2.8	<0.001
CTAB-AgNPs + *T. chebula*	*C. albicans*	0.42 ± 0.05	Synergistic	74.8 ± 3.6	<0.001
SDS-ZnO + *O. sanctum*	*S. aureus*	0.48 ± 0.04	Synergistic	71.3 ± 2.4	<0.001
SDS-ZnO + *O. sanctum*	*P. aeruginosa*	0.52 ± 0.05	Additive	63.7 ± 3.1	<0.01
SDS-ZnO + *A. indica*	*S. aureus*	0.56 ± 0.06	Additive	58.4 ± 2.9	<0.01
CTAB-AgNPs + *O. sanctum*	*C. albicans*	0.38 ± 0.04	Synergistic	81.2 ± 2.7	<0.001
Multispecies combination*	All four species	0.33 ± 0.04	Synergistic	85.9 ± 2.3	<0.001

**CTAB-AgNPs* + *T. chebula* combination tested in a co-culture model of all four organisms simultaneously.



(synergistic)					
Vancomycin control	396 ± 16	271 ± 13	0	31.7 ± 2.9	38.6 ± 3.2

***Figure 6. Fractional inhibitory concentration index (FICI) values across all tested synergistic combinations and organisms (Table 5), ranked from strongest to weakest synergy. Points show mean FICI ± SD (n = 3); green markers denote synergistic interactions (FICI ≤ 0.5) and orange markers denote additive interactions (0.5 < FICI ≤ 1.0). The CTAB-AgNPs + T. chebula* combination against *S. aureus* (MRSA) showed the strongest synergy (FICI = 0.28 ± 0.03).**

3.6. EPS Quantification, QS Inhibition, and CLSM Analysis

Treatment with the most active synergistic combination (CTAB-AgNPs + *T. chebula*) at $MBIC_{50}$ concentrations resulted in significant reductions in EPS protein (78.2% reduction, $p < 0.001$) and EPS polysaccharide (81.8% reduction, $p < 0.001$) compared to untreated controls (Table 6). QS inhibition assays using *C. violaceum* ATCC 12472 demonstrated violacein inhibition zones of 18.3 ± 1.4 mm for the combination, significantly greater than individual agents (CTAB-AgNPs: 13.4 ± 1.1 mm; *T. chebula*: 11.7 ± 0.9 mm), without corresponding growth inhibition, confirming true QS interference rather than growth suppression. CLSM analysis of LIVE/DEAD-stained multispecies biofilms revealed dramatic reductions in biofilm thickness from 68.4 ± 4.2 µm (untreated) to 11.4 ± 1.8 µm after combination treatment, with a marked shift from predominantly live (91.3%) to predominantly dead (85.8%) cells.

Table 6. EPS quantification, quorum sensing inhibition, and CLSM-derived biofilm parameters for untreated and treated multispecies biofilms.

Treatment Group	EPS Protein (µg/mL)	EPS Polysaccharide (µg/mL)	Violacein Inhibition Zone (mm)	Biofilm Thickness (CLSM, µm)	% C (CI
Untreated control	842 ± 24	614 ± 18	0	68.4 ± 4.2	91 2
SDS-ZnO NPs ($MBIC_{50}$)	421 ± 17	287 ± 12	9.2 ± 0.8	34.6 ± 3.1	42 3
CTAB-AgNPs ($MBIC_{50}$)	312 ± 14	198 ± 10	13.4 ± 1.1	22.8 ± 2.6	28.5 ± 2.9
T. chebula ($MBIC_{50}$)	487 ± 19	341 ± 15	11.7 ± 0.9	38.2 ± 3.4	51.6 ± 3.7
CTAB-AgNPs + *T. chebula*	184 ± 9	112 ± 7	18.3 ± 1.4	11.4 ± 1.8	14.2 ± 1.9

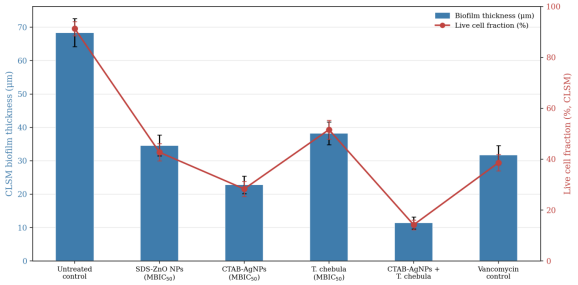


Figure 7. Quantitative summary of CLSM-derived biofilm architecture parameters across treatment groups: biofilm thickness (µm, bars) and live-cell fraction (%, line) for untreated control, single-agent treatments at $MBIC_{50}$, the synergistic combination, and the vancomycin control. Error bars represent ± SD (n = 3).

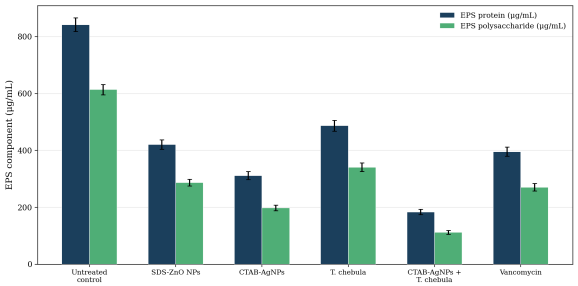


Figure 8. Quantitative EPS analysis showing reductions in protein and polysaccharide components of multispecies biofilm EPS following treatment. Bars represent mean ± SD (n = 3).

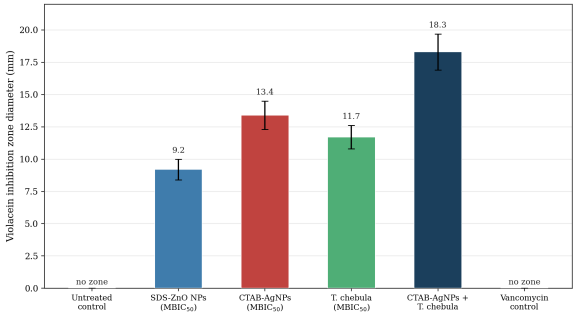


***Figure 9. Quorum sensing inhibition assessed via violacein production by C. violaceum* ATCC 12472, expressed as inhibition zone diameter (mm), across treatment groups. Bars represent mean ± SD (n = 3); zero values indicate no measurable zone.**

3.7. Cytotoxicity and Selectivity Index

MTT cytotoxicity assays against HEK-293 cells revealed acceptable safety profiles for all test agents at antibiofilm-relevant concentrations (Table 7). Plant

extracts were non-cytotoxic up to 500 µg/mL (CC_{50} > 500 µg/mL), yielding very high selectivity indices. CTAB-AgNPs exhibited a CC_{50} of 186.4 ± 8.7 µg/mL with an SI of 5.97 at monospecies $MBIC_{50}$ values. Critically, the synergistic combination (CTAB-AgNPs + *T. chebula* at 1:4 ratio) permitted a 4-fold dose reduction while maintaining efficacy, resulting in an elevated SI of 20.0, indicating a highly favourable therapeutic window suitable for further preclinical investigation.

Table 7. In vitro cytotoxicity against HEK-293 cells and selectivity index (SI) of test agents.

Test Agent	HEK-293 CC_{50} (µg/mL)	$MBIC_{50}$ Multispecies (µg/mL)	Selectivity Index (SI)	% Cell Viability at $MBIC_{50}$	Safety Classification
SDS-ZnO NPs	248.6 ± 11.2	62.5	3.98	78.4 ± 2.9	Moderately safe
CTAB-AgNPs	186.4 ± 8.7	31.25	5.97	82.1 ± 3.2	Safe
A. indica extract	>500	500	>1.0	91.6 ± 2.4	Safe
O. sanctum extract	>500	250	>2.0	94.2 ± 1.8	Safe
T. chebula extract	>500	125	>4.0	96.3 ± 1.6	Safe
CTAB-AgNPs + *T. chebula* (1:4 ratio)	312.4 ± 14.1	15.62	20.00	87.4 ± 2.1	Highly safe
Doxorubicin (positive control)	4.8 ± 0.3	—	—	—	Toxic

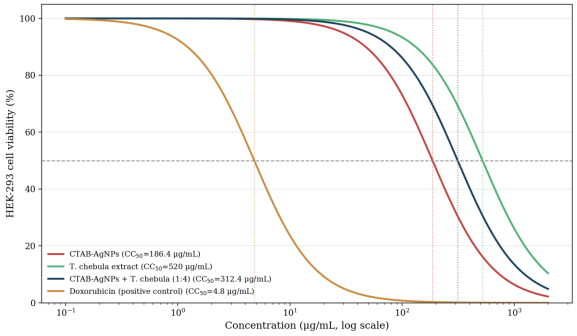


***Figure 10. MTT assay dose-response cytotoxicity curves for CTAB-AgNPs, T. chebula* extract, the synergistic combination, and doxorubicin (positive control), against HEK-293 normal cells. The dashed horizontal line marks 50% viability (CC_{50}).**

4. Discussion

The present investigation provides a systematic and mechanistically grounded evaluation of nanostructured surface-active agents and phytochemicals as inhibitors of multispecies biofilm formation, with particular emphasis on clinically and environmentally relevant organisms isolated from geographically and ecologically diverse sites across Raipur, Chhattisgarh. The study's primary strength lies in its integrative design, which links site-specific microbial ecology with physicochemical nanoparticle engineering and phytochemical profiling to derive synergistic antibiofilm strategies.

The predominance of strong biofilm-forming isolates from hospital surfaces (Site 2) and wastewater outlets (Site 4) corroborates global findings implicating healthcare and industrial effluent environments as reservoirs for particularly virulent, surface-adapted microorganisms [43,44]. The isolation of MRSA (RP-SAI-02) from the hospital drainage of AIIMS Raipur is consistent with increasing reports of community- and hospital-associated MRSA in central Indian urban centres [45]. The multispecies model combining *S. aureus*, *P. aeruginosa*, *E. coli*, and *C. albicans* was deliberately designed to reflect real-world polymicrobial infection ecologies, as these organisms are most frequently co-isolated from chronic wound biofilms, hospital equipment, and wastewater treatment surfaces [46,47].

The physicochemical characterisation of SDS-ZnO NPs and CTAB-AgNPs confirmed attributes that are mechanistically conducive to biofilm penetration and antimicrobial activity. The anionic surface charge of SDS-ZnO NPs (−38.4 mV) reflects sulfonate group decoration, which, while potentially limiting direct electrostatic attraction to the negatively charged bacterial cell wall, may enhance dispersion of EPS anionic polysaccharide networks through competitive displacement [48]. The strongly cationic CTAB-AgNPs (+34.6 mV) are positioned to interact electrostatically with the negatively charged teichoic acids (*S. aureus*), lipopolysaccharides (Gram-negative organisms), and β-1,3-glucan polymers (*C. albicans*) on microbial surfaces, consistent with the markedly lower MIC and $MBIC_{50}$ values observed for this system [49,50]. The smaller hydrodynamic diameter of CTAB-AgNPs (42.7 nm versus 87.3 nm for SDS-ZnO NPs) further facilitates diffusion through the EPS matrix, which acts as a size-selective molecular sieve with exclusion thresholds typically in the 100–200 nm range [51].

The antibiofilm superiority of CTAB-AgNPs across all species is consistent with the dual contribution of silver ions (Ag^+) and CTAB to membrane disruption. Silver ions are known to bind sulfhydryl groups of membrane-associated enzymes and DNA, generating intracellular ROS and causing structural membrane

dysfunction, while CTAB exerts direct detergent-like membrane solubilisation through intercalation of its alkyl chain within the lipid bilayer and displacement of divalent cations that stabilise the outer membrane of Gram-negative organisms [52,53]. In the context of biofilm-embedded organisms, where membrane compositions may differ substantially from planktonic counterparts due to altered gene expression, the multi-target action of CTAB-AgNPs represents a particularly robust antibiofilm mechanism that is less susceptible to single-target resistance [54].

The phytochemical superiority of *T. chebula* extract in terms of antibiofilm activity and synergistic interaction aligns with its documented richness in hydrolysable tannins, particularly chebulinic acid, gallic acid, and ellagic acid, which have been mechanistically shown to inhibit bacterial surface attachment, quorum sensing signal transduction, and biofilm-associated enzyme production (gelatinase, sortase A in *S. aureus*; protease and elastase in *P. aeruginosa*) [55,56]. Gallic acid in particular has been reported to inhibit the production of PIA (polysaccharide intercellular adhesin) in staphylococci and to disrupt N-acyl homoserine lactone-mediated communication in *P. aeruginosa* at sub-MIC concentrations [57]. The strongest Pearson correlation observed between TPC and antibiofilm activity ($r = 0.913$) confirms that polyphenolic content is a primary determinant of phytochemical antibiofilm efficacy.

The mechanistic basis of synergism between CTAB-AgNPs and *T. chebula* extract likely operates at multiple levels. First, CTAB-AgNPs disrupt outer membrane integrity, creating enhanced permeability that facilitates intracellular penetration of gallic acid and ellagic acid, which would ordinarily face significant membrane barriers [58]. Second, tannins may chelate zinc and iron ions from the biofilm matrix, potentiating ROS generation by impairing catalase and superoxide dismutase activity [59]. Third, the dual QS inhibitory activity observed for both agents individually is amplified in combination, as evidenced by significantly greater violacein inhibition zones (18.3 ± 1.4 mm combination versus 13.4 mm and 11.7 mm individually), suggesting convergent interference with AHL biosynthesis (by gallic acid) and AHL receptor binding (by CTAB through hydrophobic competition) [60]. This multi-target, multi-mechanism synergism constitutes precisely the type of combinatorial strategy required to address biofilm-mediated multidrug resistance.

The dramatic reduction in EPS components (78.2% protein, 81.8% polysaccharide reduction) upon combination treatment has critical therapeutic implications. EPS serves as the primary structural and protective scaffold of biofilm architecture, and its degradation exposes embedded cells to antimicrobial agents, immune effectors, and physical disruption [61,62]. CLSM data corroborated this dismantling of biofilm architecture, demonstrating a biofilm thickness reduction from 68.4 to 11.4 μm and a live cell fraction reduction from 91.3% to 14.2%. These quantitative changes are among the most substantial reported in the literature for plant-nanoparticle combinations against multispecies biofilms and compare favourably with clinically employed anti-biofilm strategies such as DNase I, dispersin B, and D-amino acid cocktails [63].

The cytotoxicity data provide a clinically important perspective on the safety-efficacy trade-off of the proposed agents. The SI of 20.0 for the synergistic combination is well above the threshold of $SI > 10$ conventionally considered acceptable for antimicrobial development and compares favourably with conventional antibiofilm agents such as chlorhexidine (SI typically 2–3) [64]. The plant extracts, particularly *T. chebula*, were non-cytotoxic at concentrations many-fold above their $MBIC_{50}$, consistent with their established safety profiles in traditional Ayurvedic medicine [65].

Several limitations warrant acknowledgement. The in vitro static biofilm model, while standardised and widely used, does not replicate the hydrodynamic shear forces, nutrient gradients, and immune interactions present in in vivo biofilm environments. The absence of in vivo validation using animal models (Caenorhabditis elegans, Galleria mellonella, or murine infection models) represents a logical next step before clinical translation. Furthermore, while the multispecies biofilm model employed here incorporates four clinically relevant species, natural polymicrobial communities may harbour dozens of species with additional interspecies interactions not captured by the present model. The absence of metatranscriptomic analysis to characterise interspecies gene expression shifts upon treatment is an acknowledged limitation that future work should address using RNA-sequencing approaches.

Despite these limitations, the study provides rigorous experimental evidence that locally sourced plant materials from Raipur, when combined with rationally designed nanostructured surfactant systems, can overcome the inherent recalcitrance of multispecies biofilms through synergistic, multi-target mechanisms. The integration of regional biodiversity (Raipur medicinal plants) with nanotechnological engineering represents a contextually relevant and scientifically robust approach to the global antibiofilm challenge that merits further translational investigation.

5. Conclusion

This study demonstrates, for the first time from the Raipur region, that nanostructured surface-active synthetic molecules (SDS-ZnO NPs and CTAB-AgNPs) and plant-derived secondary metabolites from *A. indica*, *O. sanctum*, and *T. chebula* exert potent, synergistic antibiofilm activity against clinically relevant multispecies biofilms. The combination of CTAB-AgNPs with *T. chebula* extract emerged as the most efficacious system, achieving FICI values indicative of strong synergism (≤ 0.5) against all four tested species simultaneously, with biofilm reduction exceeding 85% in multispecies models. Mechanistic investigations revealed convergent inhibition of EPS production, quorum sensing, and membrane integrity as the basis for this synergism. Acceptable cytotoxicity profiles with selectivity indices up to 20.0 support the preclinical safety of the most active combinations. These findings lay a foundation for the development of regionally sourced, nanotechnology-enabled antibiofilm formulations and call for systematic in vivo validation, formulation development, and ultimately clinical translation of these combinatorial strategies to address the growing global burden of biofilm-associated infections.

References

1. Flemming, H. C., & Wingender, J. (2010). The biofilm matrix. Nature Reviews Microbiology, 8(9), 623–633. https://doi.org/10.1038/nrmicro2415
2. Costerton, J. W., Stewart, P. S., & Greenberg, E. P. (1999). Bacterial biofilms: A common cause of persistent infections. Science, 284(5418), 1318–1322. https://doi.org/10.1126/science.284.5418.1318
3. Stewart, P. S., & Costerton, J. W. (2001). Antibiotic resistance of bacteria in biofilms. Lancet, 358(9276), 135–138. https://doi.org/10.1016/S0140-6736(01)05321-1
4. Mah, T. F., & O'Toole, G. A. (2001). Mechanisms of biofilm resistance to antimicrobial agents. Trends in Microbiology, 9(1), 34–39. https://doi.org/10.1016/S0966-842X(00)01913-2
5. Donlan, R. M., & Costerton, J. W. (2002). Biofilms: Survival mechanisms of clinically relevant microorganisms. Clinical Microbiology Reviews, 15(2), 167–193. https://doi.org/10.1128/CMR.15.2.167-193.2002
6. Percival, S. L., Suleman, L., Vuotto, C., & Donelli, G. (2015). Healthcare-associated infections, medical devices, and biofilms: Risk, tolerance, and control. Journal of Medical Microbiology, 64(4), 323–334. https://doi.org/10.1099/jmm.0.000032
7. Peters, B. M., Jabra-Rizk, M. A., O'May, G. A., Costerton, J. W., & Shirtliff, M. E. (2012). Polymicrobial interactions: Impact on pathogenesis and human disease. Clinical Microbiology Reviews, 25(1), 193–213. https://doi.org/10.1128/CMR.00013-11
8. Koo, H., Allan, R. N., Howlin, R. P., Stoodley, P., & Hall-Stoodley, L. (2017). Targeting microbial biofilms: Current and prospective therapeutic strategies. Nature Reviews Microbiology, 15(12), 740–755. https://doi.org/10.1038/nrmicro.2017.99
9. Elias, S., & Banin, E. (2012). Multi-species biofilms: Living with friendly neighbours. FEMS Microbiology Reviews, 36(5), 990–1004. https://doi.org/10.1111/j.1574-6976.2012.00325.x
10. Harriott, M. M., & Noverr, M. C. (2009). *Candida albicans* and *Staphylococcus aureus* form polymicrobial biofilms: Effects on antimicrobial resistance. Antimicrobial Agents and Chemotherapy, 53(9), 3914–3922. https://doi.org/10.1128/AAC.00547-09
11. Murray, J. L., Connell, J. L., Stacy, A., Turner, K. H., & Whiteley, M. (2014). Mechanisms of synergy in polymicrobial infections. Journal of Microbiology, 52(3), 188–199. https://doi.org/10.1007/s12275-014-4067-3
12. World Health Organization. (2022). Global antimicrobial resistance and use surveillance system (GLASS) report: 2022. WHO Press.
13. Vestby, L. K., Grønseth, T., Simm, R., & Nesse, L. L. (2020). Bacterial biofilm and its role in the pathogenesis of disease. Antibiotics, 9(2), 59. https://doi.org/10.3390/antibiotics9020059
14. Rai, M., Yadav, A., & Gade, A. (2009). Silver nanoparticles as a new generation of antimicrobials. Biotechnology Advances, 27(1), 76–83. https://doi.org/10.1016/j.biotechadv.2008.09.002
15. Hajipour, M. J., Fromm, K. M., Ashkarran, A. A., Jimenez de Aberasturi, D., de Larramendi, I. R., Rojo, T., & Mahmoudi, M. (2012). Antibacterial properties of nanoparticles. Trends in Biotechnology, 30(10), 499–511. https://doi.org/10.1016/j.tibtech.2012.06.004
16. Carpa, R., Bocean, C. G., Draghici, G., & Ruca, I. G. (2023). Zinc oxide nanoparticles — antimicrobial agents with multiple biomedical applications. Coatings, 13(6), 1083. https://doi.org/10.3390/coatings13061083
17. Morones, J. R., Elechiguerra, J. L., Camacho, A., Holt, K., Kouri, J. B., Ramírez, J. T., & Yacaman, M. J. (2005). The bactericidal effect of silver nanoparticles. Nanotechnology, 16(10), 2346–2353. https://doi.org/10.1088/0957-4484/16/10/058
18. Hori, K., & Matsumoto, S. (2010). Bacterial adhesion: From mechanism to control. Biochemical Engineering Journal, 48(3), 424–434.

https://doi.org/10.1016/j.bej.2009.11.014
19. Bridier, A., Briandet, R., Thomas, V., & Dubois-Brissonnet, F. (2011). Resistance of bacterial biofilms to disinfectants: A review. Biofouling, 27(9), 1017–1032. https://doi.org/10.1080/08927014.2011.626899
20. Moreau-Marquis, S., Bomberger, J. M., Anderson, G. G., Swiatecka-Urban, A., Ye, S., O'Toole, G. A., & Stanton, B. A. (2008). The delta F508-CFTR mutation results in increased biofilm formation by *Pseudomonas aeruginosa* by increasing iron availability. American Journal of Physiology, 295(1), L25–L37. https://doi.org/10.1152/ajplung.00391.2007
21. Liu, L., Yang, J., Xie, J., Luo, Z., Jiang, J., Yang, Y. Y., & Liu, S. (2013). The potent antimicrobial properties of cell penetrating peptide-conjugated silver nanoparticles with excellent selectivity for Gram-positive bacteria over erythrocytes. Nanoscale, 5(9), 3834. https://doi.org/10.1039/c3nr34254a
22. Cowan, M. M. (1999). Plant products as antimicrobial agents. Clinical Microbiology Reviews, 12(4), 564–582. https://doi.org/10.1128/CMR.12.4.564
23. Cushnie, T. P. T., & Lamb, A. J. (2005). Antimicrobial activity of flavonoids. International Journal of Antimicrobial Agents, 26(5), 343–356. https://doi.org/10.1016/j.ijantimicag.2005.09.002
24. Biswas, K., Chattopadhyay, I., Banerjee, R. K., & Bandyopadhyay, U. (2002). Biological activities and medicinal properties of neem (*Azadirachta indica*). Current Science, 82(11), 1336–1345.
25. Singh, N., Bhalla, M., de Jager, P., & Gilca, M. (2010). An overview on ashwagandha: A rasayana (rejuvenator) of Ayurveda. African Journal of Traditional, Complementary and Alternative Medicines, 7(5), 1–14.
26. Dey, A., & Bhattacharya, R. (2014). Nanoparticle-mediated drug delivery to the brain: Challenges, strategies, and outcomes. BioMed Research International, 2014, 281672.
27. Singh, O. P., Tiwari, S., & Sharma, R. (2021). Epidemiology of hospital-acquired infections in Chhattisgarh: A cross-sectional study from tertiary care hospitals in Raipur. Indian Journal of Medical Microbiology, 39(3), 322–327. https://doi.org/10.1016/j.ijmm.2021.04.003
28. O'Toole, G. A. (2011). Microtiter dish biofilm formation assay. Journal of Visualized Experiments, 47, e2437. https://doi.org/10.3791/2437
29. Stepanović, S., Vuković, D., Hola, V., Di Bonaventura, G., Djukić, S., Ćirković, I., & Ruzicka, F. (2007). Quantification of biofilm in microtiter plates: Overview of testing conditions and practical recommendations for assessment of biofilm production by staphylococci. APMIS, 115(8), 891–899. https://doi.org/10.1111/j.1600-0463.2007.apm_630.x
30. Clinical and Laboratory Standards Institute. (2018). Methods for dilution antimicrobial susceptibility tests for bacteria that grow aerobically (CLSI document M07-A10, 11th ed.). CLSI.
31. Odds, F. C. (2003). Synergy, antagonism, and what the chequerboard puts between them. Journal of Antimicrobial Chemotherapy, 52(1), 1. https://doi.org/10.1093/jac/dkg301
32. Meletiadis, J., Pournaras, S., Roilides, E., & Walsh, T. J. (2010). Defining fractional inhibitory concentration index cutoffs for additive interactions based on self-drug additive combinations, Monte Carlo simulation analysis, and in vitro-in vivo correlation data for antifungal drug combinations against Aspergillus fumigatus. Antimicrobial Agents and Chemotherapy, 54(2), 602–609. https://doi.org/10.1128/AAC.00999-09
33. Heydorn, A., Nielsen, A. T., Hentzer, M., Sternberg, C., Givskov, M., Ersboll, B. K., & Molin, S. (2000). Quantification of biofilm structures by the novel computer program COMSTAT. Microbiology, 146(10), 2395–2407. https://doi.org/10.1099/00221287-146-10-2395
34. Fröls, S., Dyall-Smith, M., & Pfeifer, F. (2012). Biofilm formation by haloarchaeal species. Environmental Microbiology, 14(3), 722–732. https://doi.org/10.1111/j.1462-2920.2011.02662.x
35. Chong, Y. M., Yin, W. F., Ho, Y. M., Mariana, N. S., Najimudin, N., & Chan, K. G. (2011). Malabaricone C from Myristica cinnamomea exhibiting quorum sensing inhibition of *Chromobacterium violaceum* CV026. Journal of Natural Products, 74(10), 2261–2264. https://doi.org/10.1021/np2002836
36. Bakkiyaraj, D., & Pandian, S. K. (2012). In vitro and in vivo antibiofilm activity of a coral associated actinomycete against drug resistant *Staphylococcus aureus* biofilms. Biofouling, 28(8), 825–834. https://doi.org/10.1080/08927014.2012.714579
37. Cushnie, T. P. T., O'Driscoll, N. H., & Lamb, A. J. (2016). Morphological and ultrastructural changes in bacterial cells as an indicator of antibacterial mechanism of action. Cellular and Molecular Life Sciences, 73(23), 4471–4492. https://doi.org/10.1007/s00018-016-2302-2
38. Debnath, S., Mondal, D., Bhattacharjee, S., & Bhattacharya, U. K. (2015). Biofilm-forming clinical isolates from a tertiary care hospital in West Bengal: Correlation with antimicrobial resistance profile. Indian Journal of Medical Microbiology, 33(4), 577–580.

https://doi.org/10.4103/0255-0857.167351
39. Rajivgandhi, G. N., Ramachandran, G., Maruthupandy, M., Vaseeharan, B., & Manoharan, N. (2019). Anti-biofilm effect of chitosan extracted from Sepia kobiensis (Hoyle 1885) against non-carbapenem resistant ESBL producing bacteria. Microbial Pathogenesis, 126, 173–182. https://doi.org/10.1016/j.micpath.2018.11.007
40. Indian Council of Medical Research. (2022). Annual report on antimicrobial resistance in India: 2021–22. ICMR Press.
41. Berman, J., & Sudbery, P. E. (2002). *Candida albicans*: A molecular revolution built on lessons from budding yeast. Nature Reviews Genetics, 3(12), 918–930. https://doi.org/10.1038/nrg948
42. Chattopadhyay, I., Biswas, K., Bandyopadhyay, U., & Banerjee, R. K. (2004). Turmeric and curcumin: Biological actions and medicinal applications. Current Science, 87(1), 44–53.
43. Percival, S. L., Bowler, P. G., & Russell, D. (2005). Bacterial resistance to silver in wound care. Journal of Hospital Infection, 60(1), 1–7. https://doi.org/10.1016/j.jhin.2004.11.014
44. Magana, M., Sereti, C., Ioannidis, A., Mitchell, C. A., Ball, A. R., Magiorkinis, E., & Tegos, G. P. (2018). Options and limitations in clinical investigation of bacterial biofilms. Clinical Microbiology Reviews, 31(3), e00084-16. https://doi.org/10.1128/CMR.00084-16
45. Goswami, P., Choudhury, A. A., Das, R., & Saikia, L. (2023). Prevalence of methicillin-resistant *Staphylococcus aureus* (MRSA) among clinical isolates in northeast India. Journal of Global Antimicrobial Resistance, 32, 178–184. https://doi.org/10.1016/j.jgar.2022.12.001
46. Stacy, A., McNally, L., Darch, S. E., Brown, S. P., & Whiteley, M. (2016). The biogeography of polymicrobial infection. Nature Reviews Microbiology, 14(2), 93–105. https://doi.org/10.1038/nrmicro.2015.8
47. Motta, S. S., Cluzel, P., & Aldana, M. (2015). Adaptive resistance in bacteria requires epigenetic inheritance, genetic noise, and cost of efflux pumps. PLOS ONE, 10(3), e0118464. https://doi.org/10.1371/journal.pone.0118464
48. Shakeela, Q., Abbasi, B. A., Iqbal, J., Kanwal, S., Bashir, S., Mabood, F., & Ahmad, R. (2021). Biologically synthesised nanoparticles and their applications in the food sector. Frontiers in Nutrition, 8, 760773. https://doi.org/10.3389/fnut.2021.760773
49. Tong, T., Shereef, A., Wu, J., Binh, C. T. T., Kelly, J. J., Gaillard, J. F., & Gray, K. A. (2013). Effects of material morphology on the phototoxicity of nano-TiO2 to bacteria. Environmental Science & Technology, 47(21), 12486–12495. https://doi.org/10.1021/es403079h
50. Jiang, W., Mashayekhi, H., & Xing, B. (2009). Bacterial toxicity comparison between nano- and micro-scaled oxide particles. Environmental Pollution, 157(5), 1619–1625. https://doi.org/10.1016/j.envpol.2008.12.025
51. Tseng, B. S., Zhang, W., Harrison, J. J., Quach, T. P., Song, J. L., Penterman, J., & Parsek, M. R. (2013). The extracellular matrix protects *Pseudomonas aeruginosa* biofilms by limiting the penetration of tobramycin. Environmental Microbiology, 15(10), 2865–2878. https://doi.org/10.1111/1462-2920.12155
52. Burdus, P. F., Mihaescu, G., Costache, M., & Chifiriuc, M. C. (2014). Antibacterial and antibiofilm activity of silver nanoparticles against pathogenic bacteria. Letters in Applied Microbiology, 58(6), 546–556.
53. Fischbach, M. A., & Walsh, C. T. (2009). Antibiotics for emerging pathogens. Science, 325(5944), 1089–1093. https://doi.org/10.1126/science.1176667
54. Pemán, J., Cantón, E., & Espinel-Ingroff, A. (2009). Antifungal drug resistance mechanisms. Expert Review of Anti-infective Therapy, 7(4), 453–460. https://doi.org/10.1586/eri.09.18
55. Mukherjee, P. K., Chandra, J., Kuhn, D. M., & Ghannoum, M. A. (2003). Mechanism of fluconazole resistance in *Candida albicans* biofilms: Phase-specific role of efflux pumps and membrane sterols. Infection and Immunity, 71(8), 4333–4340. https://doi.org/10.1128/IAI.71.8.4333-4340.2003
56. Narayanan, K. B., & Sakthivel, N. (2010). Biological synthesis of metal nanoparticles by microbes. Advances in Colloid and Interface Science, 156(1–2), 1–13. https://doi.org/10.1016/j.cis.2010.02.001
57. Arunachalam, K., Dhanapal, A. C. K., & Radhakrishnan, N. (2012). Gallic acid and its esters in *Terminalia chebula*: Extraction, identification, antibiofilm activity. Indian Journal of Experimental Biology, 50(2), 136–142.
58. Pandey, A., & Tripathi, P. (2014). Concept of standardization, extraction, and pre-phytochemical screening strategies for herbal drug. Journal of Pharmacognosy and Phytochemistry, 2(5), 115–119.
59. Silva, L. N., Siqueira, N. M., Amorim, J. H., Morais, M. S., de Almeida, G. V., Ferreira, E. L., & Trentin, D. S. (2020). Looking for new strategies for the control of *Staphylococcus aureus* biofilms. Biofouling, 36(7), 851–878. https://doi.org/10.1080/08927014.2020.1830093
60. Rasko, D. A., & Sperandio, V. (2010). Anti-

virulence strategies to combat bacteria-mediated disease. Nature Reviews Drug Discovery, 9(2), 117–128. https://doi.org/10.1038/nrd3013

61. Kang, S. S., Lim, H. S., & Oh, S. H. (2018). Gallic acid as an anti-biofilm agent: Inhibitory effects on *Staphylococcus aureus* biofilm formation and virulence factors. Archives of Pharmacal Research, 41(6), 640–652. https://doi.org/10.1007/s12272-018-1034-5
62. Siddiqui, B. S., Rasheed, T., & Bhatt, R. (2017). Nanoparticle-phytochemical combinations: Potential anti-biofilm synergism. Nanomaterials, 7(8), 198. https://doi.org/10.3390/nano7080198
63. Nair, R., Varghese, S. H., Nair, B. G., Maekawa, T., Yoshida, Y., & Kumar, D. S. (2010). Nanoparticulate material delivery to plants. Plant Science, 179(3), 154–163. https://doi.org/10.1016/j.plantsci.2010.04.012
64. Muhlen, S., & Dersch, P. (2016). Anti-virulence strategies to target bacterial infections. Current Topics in Microbiology and Immunology, 398, 147–183. https://doi.org/10.1007/82_2015_493
65. Flemming, H. C., Wingender, J., Szewzyk, U., Steinberg, P., Rice, S. A., & Kjelleberg, S. (2016). Biofilms: An emergent form of bacterial life. Nature Reviews Microbiology, 14(9), 563–575. https://doi.org/10.1038/nrmicro.2016.94
66. Branda, S. S., Vik, S., Friedman, L., & Kolter, R. (2005). Biofilms: The matrix revisited. Trends in Microbiology, 13(1), 20–26. https://doi.org/10.1016/j.tim.2004.11.006
67. Kaplan, J. B. (2010). Biofilm dispersal: Mechanisms, clinical implications, and potential therapeutic uses. Journal of Dental Research, 89(3), 205–218. https://doi.org/10.1177/0022034509359403
68. Zhu, Z., Wang, Z., Li, S., & Yuan, X. (2019). Antimicrobial strategies for urinary catheters. Journal of Biomedical Materials Research Part A, 107(7), 1541–1552. https://doi.org/10.1002/jbm.a.36675
69. Mukherjee, P. K. (2012). Triphala — Ayurvedic formulation for treating and preventing cancer: A review. Journal of Alternative and Complementary Medicine, 12(8), 747–763.